A scaling approach to size effect modeling of J_c CDF for 20MnMoNi55 reactor steel in transition temperature region

Sreten Mastilovic [a,*] , Branislav Djordjevic[b], Aleksandar Sedmak[c]

[a] *Institute for Multidisciplinary Research, University of Belgrade, Kneza Viseslava 3, 11030 Belgrade, Serbia*
[b] *Innovation Center of Faculty of Mechanical Engineering, Kraljice Marije 16, 11120 Belgrade, Serbia*
[c] *Faculty of Mechanical Engineering, University of Belgrade, Kraljice Marije 16, 11120 Belgrade, Serbia*

ABSTRACT

Ever since the 1980s there is a sustained interest in the size effect, as one of the most pronounced consequences of fracture mechanics. In the present study, the investigation of the size effect is focused on estimation of the Weibull cumulative distribution function (CDF) of the critical value of the *J*-integral (J_c) in the transition temperature region under constraint of a small statistical sample size. Specifically, the J_c experimental data correspond to the C(T) specimen testing of the reactor pressure-vessel steel 20MnMoNi55 at only two geometrically-similar sizes. Thus, a simple approximate scaling algorithm has been developed to tackle the effect of the C(T) specimen size on the J_c CDF under these circumstances. Due to the specific form of the two-parameter Weibull CDF, $F(J_c \mid \beta, \eta)$, the scaling procedure is applied according to a two-step scheme. First, the J_c-scaling is performed to ensure the approximate overlap of the points that correspond to the CDF value $F(J_c = \eta) = 1 - 1/e \approx 0.632$ for different C(T) specimen widths (W), which assumes $\eta \cdot W^{\kappa} = \text{const}$. Second, the F-scaling is performed to ensure the equality of the slopes of the CDF in the scaled ($F \cdot W^{\xi}$ vs. $J_c \cdot W^{\kappa}$) space. The objective of the sketched approach is to obtain a size-dependent J_c CDF that encapsulates a reasonably conservative data extrapolation.

Key words: size effect, scaling, Weibull distribution, cumulative distribution function, lower bound

1. Introduction

In the traditional plasticity theory, the strength of geometrically-similar structures does not exhibit the size effect. Nonetheless, the size effect emerges from comparison of different sizes of geometrically-similar structures made of brittle materials, especially at extremely low temperatures when the plasticity mechanisms are largely suppressed. This applies especially to metals embrittled by fatigue or—more importantly in the present case—for the reactor (pressure-vessel) steel embrittled by radiation. Historically, the glaring necessity that the structural analysis ought to capture the size effect has been among few most compelling reasons prompting design engineers to integrate fracture mechanics theory into the engineering standards and codes [1].

Metallic structures exposed to environmental embrittlement and temperatures in the brittle-to-ductile transition region or lower, fail typically due to propagation of a macroscopic crack (the plastic collapse being unlikely under those circumstances). The cleavage failure occurs as soon as the dominant microcrack (or microflaw) reaches macroscopic dimensions and "percolates" through the structure. The mechanics of low-temperature metallic failures favors, so called, statistical size effect[1] described traditionally by the weakest link Weibull statistics. Therefore, the Weibull distribution, in two- and three-parameter forms, has been widely utilized for empirical and statistical characterization of cleavage fracture toughness of reactor steels.

During the last four decades the size effect has been studied intensively and, accordingly, an extensive theoretical, experimental and computational literature is available. While admitting an unintentional bias of authors from their personal interests and research backgrounds, the best known models likely include Size Effect Law [1, 2] and Multifractal Scaling Law [3] focused on the size-effect modeling of strength *fitted* to experimental data sets. The lattice models are early recognized as computational tools well suited for the size effect investigation (e.g., [4-8]). More resent references are, not surprisingly, focused on quasibrittle solids; frequently concrete [8-11]. As pointed out by Bažant and coauthors [11], "for perfectly ductile and perfectly brittle structures, the empirical approach is sufficient because the cumulative distribution function (CDF) of random material strength is known and fixed." The size effects of quasibrittle fracture stem from the statistical expectation that increase of material volume results in increase of the number of "weak links and hot spots" [8]. Most notable, in this regard, are inhomogeneities of the size not negligible compared with the structural dimensions [11]. Consequently, the increase of the size-effect sensitivity is typically accompanied with the increase of the representative volume element (whose size *is*, for the plastic materials, negligible in comparison with the structural dimensions).

The brittle fracture, especially at cryogenic temperatures, is characterized by a pronounced aleatory variability. Consequently, sample-to-sample variations are very strong (especially for small specimen) and a statistical approach is useful. The Weibull theory is one of the first size-effect theories of the strength of materials that is purely statistical [12]. The Weibull statistics is based on the weakest-link theory, which aptly emphasizes the virtual absence of stress redistribution during failure accompanying the innately brittle behavior. Due to the low temperature addressed in the present study (-60 C and -90 C [13]), plasticity mechanisms and stress redistribution are largely suppressed and the cleavage fracture that nucleates at the weakest spot propagates mostly unobstructed, which results in catastrophic failure of the whole specimen. Consequently, the nature of the size effect appears inherently statistical – that is, of the kind traditionally described by the Weibull distribution (e.g., [14-16]).

Among numerous statistical studies of cleavage fracture toughness of ferritic steels that make use of the Weibull statistics, four arguably the most prominent approaches are briefly mentioned hereinafter followed by a sample of recent developments. The empirical approach by Landes and coworkers [16] was based on the assumption that the cleavage fracture toughness was controlled by the weakest link at the crack front. This approach is extensively used to this day (e.g., [13]). The two-parameter Weibull distribution, they proposed as

* Corresponding author.
E-mail address: misko.mastilovic@imsi.bg.ac.rs (S. Mastilovic).

[1] Not to be confused with *the fracture mechanics size effect* due to the release of the accumulated structural energy into the process zone of the decisive macrocrack; which is, arguably, the most important manifestation of fracture phenomena from the engineering standpoint [1].

the failure probability, is the corner stone of the present study as well. (Landes and coauthors [17] also advanced a method for determining a lower-bound fracture toughness value from the result of a *single* test in the transition temperature region for ferritic steels.) The Beremin local model [18, 19] was developed in attempt to pursue a statistical approach to the inherently stochastic fracture by taking into account the salient micromechanical features in the process. Many aspects of this influential model, its shortcomings and necessary corrections, were discussed recently by Qian et al. [20]. Wallin [21, 22] performed more detailed analysis which resulted in the two-parameter Weibull model known as the Master Curve model. This approach, similarly to the Beremin model, belongs to the local approach category. It was based on the weakest-links premise and application of the cleavage micromechanics. The model involved very complex procedures of the experimental data treatment. The master curve studies have been incorporated into the ASTM standards and code cases and the IAEA guidelines (e.g., [23-25]). The Prometey model [25, 26], in its advanced form, involved very complex statistical treatment of micromechanics assuming that both the microcrack nucleation and the microcrack propagation were driven by stochastic parameters. The model development involved "intricate series of assumptions and formulations" [20]. Lei [27, 28] offered an influential critical assessment of the three above-mentioned local models, with emphasis on physical justification of the widely adopted selection of Weibull model parameters. Lei also proposed an original statistical model of the cleavage fracture toughness and compared it with the three above-mentioned models. Finally, Meshii [29] recently stressed the problems of the ASME E 1921 master curve [23] with characterization of fracture toughness temperature dependence. An alternative master curve model was proposed, which captured the statistical distribution of fracture toughness, based on the C(T) (compact tension) experimental data, and included both temperature and size effects.

The objective of the present investigation is to develop an expression for the Weibull CDF for the critical value of the J-integral (J_c) for ferritic steels in the ductile-to-brittle transition temperature region, which takes into account the C(T) specimen size (Fig. 1).[2] Under the constraint of a small statistical sample size, this expression should provide a reasonably conservative extrapolation of the Weibull J_c CDF away from the available experimental data. The experimental data used correspond to the C(T) specimen of two effective widths $W = \{50, 100\}$ [mm] [13]. An original scaling algorithm has been developed and presented in the next section to meet the stated objective. Due to the specific form of the two-parameter Weibull CDF $F(J_c \mid \beta, \eta)$, this algorithm is applied according to a two-step scheme outlined below.

2. Scaling procedure

Historically, scaling theories have been originally developed in attempt to describe critical phenomena and physics of phase transitions. The scaling algorithm proposed herein is inspired by Mandelbrot's idea of "a unifying description of natural phenomena which are not uniform but still obey simple power laws" of the form $M \propto L^D$, where L is a characteristic linear dimension [32]. The effective width, W, of the C(T) specimen (Fig. 1) is considered that characteristic dimension throughout this study. Nonetheless, the three-dimensional (3-D) geometric similarity of the C(T) specimens used in the testing program reported by Djordjevic et al. [13, 33], implies that W/B = const., where B is the net C(T) specimen thickness. Therefore, the results obtained herein can be straightforwardly rewritten with B as the characteristic dimension. Furthermore, the used sequential scaling somewhat resembles the Krajcinovic and Rinaldi's two-step application of the Family–Vicsek scaling law used to model size-dependent fracture in quasibrittle solids [34, 35]. The notable difference is that, except for the special case of the size-independent Weibull modulus β, it is impossible to achieve the overlap of various Weibull CDF curves.

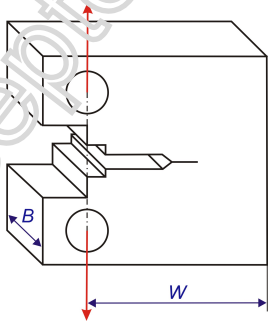

Fig. 1. Compact tension (CT) specimen with indicted effective width (W) and thickness (B).

2.1 Some basic relationships of the Weibull CDF

The starting point in the present analysis is the two-parameter Weibull CDF:

$$F(J \mid \beta, \eta) = 1 - \exp\left[-\left(\frac{J}{\eta}\right)^{\beta}\right]; \qquad J \geq 0;\ \beta, \eta \in \Re^{+} \tag{1}$$

where η and β are, respectively, the scale parameter and the Weibull modulus (shape parameter) [36] and the symbol J is used for brevity hereinafter instead of J_c. The Weibull parameters η and β are material constants sensitive to the specimen preparation, surface condition and temperature [37].

[2] The ferritic steel DIN 20MnMoNi55 is frequently used to study cleavage fracture at subzero temperatures due to its usage in demanding industrial applications (e.g., [15, 30]). Actually, development of probabilistic fracture mechanics is closely related to, if not driven by, requirements of nuclear industry [31].

The proposed scaling procedure involves the derivative of the Weibull CDF (the slope in F-J space):

$$\frac{dF(J)}{dJ}=\frac{\beta}{\eta}\left(\frac{J}{\eta}\right)^{\beta-1}\exp\left[-\left(\frac{J}{\eta}\right)^{\beta}\right]\equiv f(J\mid\beta,\eta) \tag{2}$$

which equals, by definition, the probability density function (PDF), $f(J)$. Furthermore, it is of interest to determine the slope (2) that corresponds to the inflection point of the Weibull CDF, defined by:

$$\left.\frac{d^2F}{dJ^2}\right|_{J=J_{\Pi}}=\left(\frac{\beta}{\eta}\right)^2\left(\frac{J_{\Pi}}{\eta}\right)^{\beta-2}\exp\left[-\left(\frac{J_{\Pi}}{\eta}\right)^{\beta}\right]\left[1-\frac{1}{\beta}-\left(\frac{J_{\Pi}}{\eta}\right)^{\beta}\right]=0 \tag{3}$$

where subscript Π designates the inflection point. (Obviously, the CDF inflection point, defined by Eq. (3), corresponds to the PFD maximum value.) The inflection point coordinate

$$\frac{J_{\Pi}}{\eta}=\left(1-\frac{1}{\beta}\right)^{\frac{1}{\beta}} \tag{4}$$

follows from Eq. (3) as the only non-trivial solution. After a straightforward derivation, the Weibull CDF slope (2) at the inflection point (4) is obtained in the following form:

$$S=\left.\frac{dF(J)}{dJ}\right|_{J=J_{\Pi}}=\frac{1}{\eta}\Xi(\beta)=f(J)|_{J=J_{\Pi}}=f_{\max} \tag{5}$$

where

$$\Xi(\beta)=\beta\left(1-\frac{1}{\beta}\right)^{1-\frac{1}{\beta}}\exp\left[-\left(1-\frac{1}{\beta}\right)\right] \tag{6}$$

is dubbed herein the shape function and illustrated in Fig. 2.

Clearly, Eq. (5) reaffirms that the Weibull CDF slope at the inflection point corresponds to the PDF maximum.

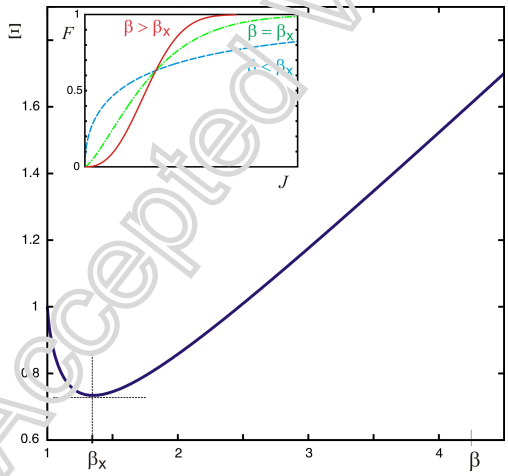

Fig. 2. Functional dependence of the shape function Ξ (6) on the Weibull modulus β. Inset: the typical shapes of the CDF for various values of the Weibull modulus illustrate that the characteristic sigmoid shape is obtained for $\beta > \beta_{\times} \approx 1.35$. (Note the existence of the minimum $\Xi_{\min} = 0.73$.)

2.2 Two-step scaling scheme

The same basic relationships derived in the preceding section are revisited herein in the scaled space ($F{\cdot}W^{\xi}$ vs. $J{\cdot}W^{\kappa}$). The motivation is that the gist of the present size-effect investigation rests upon the two scaling premises:

(i) The J-scaling condition

$$\eta_{*}=\eta\cdot W^{\kappa}=const. \tag{7}$$

which defines the size-independent Weibull scale parameter η_{*} in the scaled space ($F{\cdot}W^{\xi}$ vs. $J{\cdot}W^{\kappa}$) (Fig. 3) that feeds directly into the CDF (1), and

(ii) The F-scaling condition

$$S_{*}=S\cdot W^{\xi}=const. \tag{8}$$

which defines the common CDF slope in the scaled space (Fig. 3c), which scales with the PDF maxima.

It should be noted that Eq. (7), for positive values of the scaling parameter κ, implies that

$$\eta_\infty \equiv \lim_{W\to\infty} \eta(W) = 0 \tag{9}$$

Needless to emphasize, this is a special case since, in general, the limit value of the Weibull scale parameter corresponding to the infinite specimen ($\eta_\infty > 0$) needs to be established based on the experimental data. The limit value η_∞ is a measure of the brittleness of the system. This will be discussed later, for time being Eq. (9) holds.

Thus, the derivation of the CDF slope in the scaled space ($F\cdot W^\xi$ vs. $J\cdot W^\kappa$) yields

$$S_* = \left.\frac{dy}{dx}\right|_{x=x_\Pi} = \frac{1}{\eta_*}\,\Xi(\beta)\,W^\xi \tag{10}$$

In the course of this derivation, it is convenient to use the change of variables $y = F\cdot W^\xi$ and $x = J\cdot W^\kappa$, which results in the unaltered functional dependence of the inflection-point coordinate in the scaled space upon the Weibull modulus

$$\frac{x_\Pi}{\eta_*} = \left(1-\frac{1}{\beta}\right)^{\frac{1}{\beta}} \tag{11}$$

A couple of observation could be made based on Eq. (10). First, the Weibull scale parameter in the scaled space is size-independent, $\eta_* = \text{const}$. (Fig. 3b), by virtue of the *J*-scaling condition (7). (Recall that the *J*-scaling along the horizontal axis is performed to ensure the overlap of the E-points[3] for C(T) specimen widths (W), which implies Eq. (7).) Second, the CDF slope in the scaled space $F\cdot W^\xi$ vs. $J\cdot W^\kappa$ is also size-independent (Fig. 3c) by virtue of the *F*-scaling condition, $S_* = \text{const}$. (8). (Recall that the *F*-scaling along the vertical axis is performed to ensure the overlap of the inflection-point slopes for all W.) Consequently, it follows from Eq. (10) that

$$\Xi(\beta)\,W^\xi = const. \tag{12}$$

Also note that the PDF maximum *scales* with the common CDF slope in the scaled space

$$f_{\max} = W^{\kappa-\xi}\,S_* \tag{13}$$

The value of shape function Ξ

$$\Xi\left(\beta\,|W,\xi\right) = S_*\,\eta_*\,W^{-\xi} \tag{14}$$

can be calculated for each particular specimen dimension W, once the scaling parameter ξ and the corresponding CDF slope S_* are evaluated from Fig. 3c.

Finally, the Weibull modulus $\beta(W, \xi)$ can be determined graphically from Fig. 2 once the value of $\Xi\,(\beta \mid W, \xi)$ is known.

Eventually, the Weibull CDF can be written in the form

$$F\left(J\mid\beta,\eta\right) = 1-\exp\left\{\left(\frac{J\cdot W^\kappa}{\eta_*}\right)^{\beta(W,\xi)}\right\} \tag{15}$$

that takes into account the effect of the specimen size dimension (specifically, the effective width). As stressed already, due to the 3-D geometrical similarity of the C(T) specimen used, $W = 2.5\cdot B$ [13], it is straightforward to represent the size effect of Eq. (15) in terms of the thickness B if preferable.

Notably, the scaling parameters κ and ξ, resulting from the use of the scaling algorithm outlined above, are the materials parameters in the same way as the Weibull CDF parameters β and η. They should also be sensitive to the specimen preparation, surface condition and temperature. The constants η_* and S_* are model parameters dependent upon κ and ξ. Admittedly, they do not have a physical interpretation but are simply outcomes of the experimental data fitting (in the same manner as β and η).

Importantly, Eq. (15) is derived assuming that the limit defined by Eq. (9) holds. In general case the Weibull CDF (15) can be re-written in the form

$$F\left(J\mid\beta,\eta\right) = 1-\exp\left\{\left(\frac{J\cdot W^\kappa}{\eta_* + \eta_\infty W^\kappa}\right)^{\beta(W)}\right\} \tag{16}$$

that takes into account $\eta_\infty > 0$. Determination of η_∞ requires at least three C(T) specimen sizes. If only two sizes are available from the C(T) testing (like in the numerical example that follows), Eq. (15) provides either a reasonable estimate (in the interpolation region) or a conservative lower bound (in the extrapolation regions) for Eq. (16) for almost the entire size range of practical interest as illustrated in Fig. 4. This general form of the J_c CDF is equivalent to the size effect modeling of the Weibull scale parameter

$$\eta(W) = \eta_\infty + \eta_*\cdot W^{-\kappa} \tag{17}$$

The scaling form in terms of the system size (17) is well known from physics of phase transitions and critical phenomena [32, 38]. Notably, it can be argued that every test point corresponding to the J_c CDF inherently represents a critical point corresponding to the damage-fragmentation phase transition along the lines of argument advanced in [39].

[3] The E-point designation is introduced for clarification of Fig. 3. These points are defined by the cumulative probability $F(J = \eta) = 1 - 1/e \approx 0.632$ for different effective widths of the C(T) specimen.

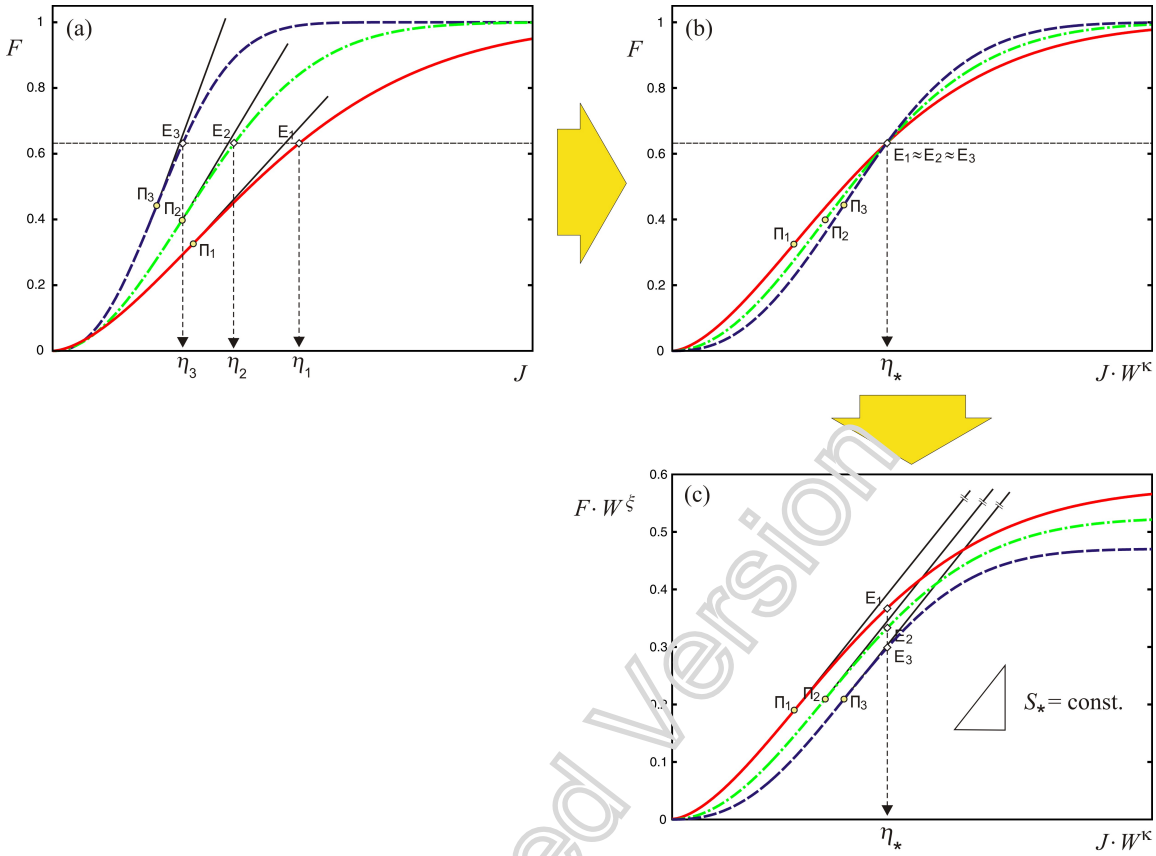

Fig. 3. Schematics of the two-step scaling algorithm demonstrated with three different system sizes.

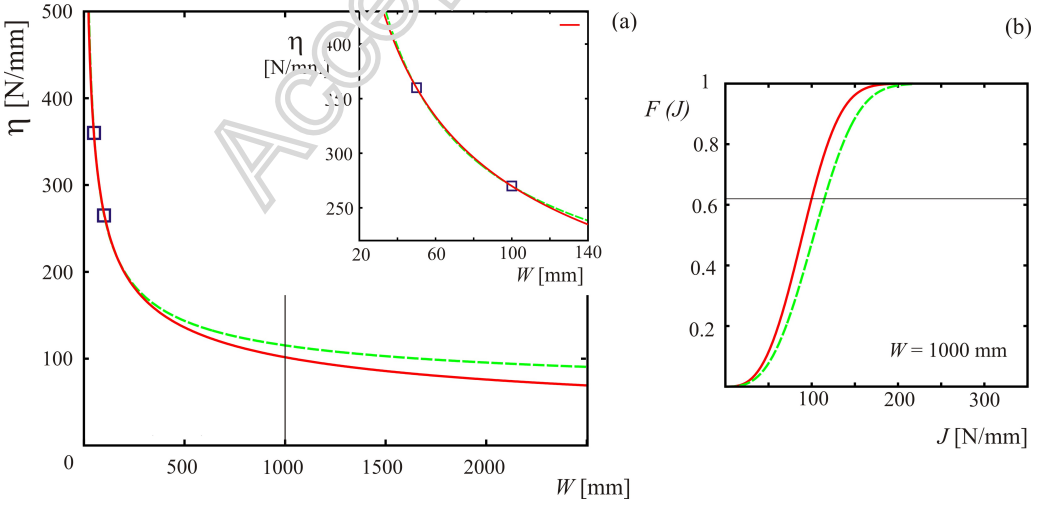

Fig. 4. (a) Dependence of the Weibull scale parameter on the C(T) specimen effective width. The square symbols mark two data points available from experiments [13]. The solid red line marks the limit case $\eta_\infty = 0$ described by Eq. (7). The dashed green line is an example of a more general case, $\eta_\infty = 50$ N/mm, corresponding to Eq. (16). (Note that the difference between two curves is artificially exaggerated in the inset to improve visibility.) (b) The solid red line represents the lower bound for the dashed green line which provides a conservative estimate for the J_c CDF for large W; an example for a rather large specimen size ($B = W/2.5 = 400$ mm).

A careful examination of Fig. 4, reveals that Eqs. (7) and (15) provide, respectively, lower bounds for more general predictions based on Eqs. (17) and (16) in the regions of extrapolation. The detail emphasized in the inset of Fig. 4a reveals that, as expected, Eq. (7) cannot represent the lower bound for Eq. (17) between the two test data points (in the interpolation region) as well, but the two curves are barely distinguishable in spite of the distance exaggeration applied in the inset to promote visibility. For all practical purposes, the two curves virtually overlap in the interpolation region and somewhat beyond. As the specimen size increases, the two curves increasingly diverge as expected. Nonetheless, the main panel of Fig. 4a illustrates that, for the range of C(T) specimen sizes commonly used in experiments, the difference is hardly noticeable. Finally, in view of the example shown in Fig. 4, it could be argued that, bearing in mind the inherently strong data scatter [13, 33], Eqs. (7) and (15) provide very reasonable CFD estimates well over the range of sizes that can be accurately tested (up to the thickness $B \approx 300 \div 400$ mm) and useful lower-bounds somewhat beyond. The importance of having the reasonably-conservative lower bounds in the data extrapolation range cannot be exaggerated bearing in mind that number of valid tests obtained with miniature specimens is substantially reduced when compared with similar tests conducted on standard specimens [40].

It should be noted that the smaller the size of the statistical sample, the more difficult is to use the above-mentioned approach directly since the graphical scaling of "few and far between" experimental data points may not be sufficiently revealing. In that case, it is useful to fit first the CDF (1) for available data sets (for all Ws), and to use these curves for the scaling guidance. In that case, Eqs. (7) and (12) could be used as a guidance to estimate the scale parameters

$$\kappa = \log_{\left(\frac{W_{i+1}}{W_i}\right)}\left(\frac{\eta_i}{\eta_{i+1}}\right), \quad \xi = \log_{\left(\frac{W_{i+1}}{W_i}\right)}\left[\frac{\Xi(\beta_i)}{\Xi(\beta_{i+1})}\right] \tag{18}$$

obtained for (among) the available data-set pair(s). (For the general case of $\eta_\infty > 0$, the Weibull scale parameter η in Eq. $(18)_1$ should be replaced by the difference $\eta - \eta_\infty$.)

Notably, Eq. $(18)_2$ reveals that *if* the Weibull modulus β is size-independent to begin with, the F-scaling is unnecessary ($\xi = 0$) since the Weibull CDFs for various specimen overlap upon the J-scaling.

3. Numerical example and discussion of results

The two-step scaling algorithm outlined above is now used to develop expression (15) for the Weibull J_c CDF for the reactor steel 20MnMoNi55. The experimental data for the C(T) test at temperature -60 °C, depicted in Fig. 5a, is obtained from [13].

First, it is opportune to examine visually the experimental data points in Fig. 5a. The statistical sample is notably small: {14, 12} data points are available for the C(T) specimen with dimensions $W = \{50, 100\}$ [mm] and $B = W / 2.5$ (the later implying the 3-D geometrical similarity). The adverse effects of the small size of the statistical sample are especially notable for the larger specimen, $W = 100$ mm, where 12 experimental data points show a strong scatter and barely suggest the characteristic sigmoid approach to the upper horizontal asymptote (the inset of Fig. 2 for $\beta > \beta_\times$); especially for the J values corresponding to the large distribution tail. This is vexing, considering that the Weibull distribution is widely applied to random phenomena exactly for its extreme value behavior [7].[4] (This pronounced sensitivity to the statistical sample size is typical for the cumulative probability plots.) Consequently, as discussed previously, the experimental data are first fitted with the CDF (1) to provide guidance and facilitate the scaling procedure. Eqs. (18) are also used for the same purpose.

Since only two experimental data sets, $W = \{50, 100\}$ [mm], are available, the J-scaling (to be performed) is limited to determination of the conservative CDF estimate (15). Thus, $\eta_* = 1850$ Nmm$^{-\kappa}$ is determined by using $\kappa = 0.42$ as shown in Fig. 5b.[5] Since the inflection-point slopes in Fig. 5b are obviously different, the corresponding Weibull moduli are different, and the F-scaling is necessary ($\xi \neq 0$). The parallel CDF slopes in the scaled space ($F \cdot W^\xi$ vs. J) are obtained for $\xi = -0.14$ as illustrated in Fig. 5c (S_* = const.= 0.00024 mm$^{1-\kappa+\xi}$/N). Thus, the two-step scaling scheme for the given data sets results in $\kappa = 0.42$, $\xi = -0.14$, $\eta_* = 1850$ Nmm$^{-0.58}$, and $S_* = 0.00024$ mm$^{0.72}$/N. Obviously, the problem involving only two C(T) specimen sizes is deterministic and the optimization of the scaling parameter values (κ and ξ) is unnecessary.

The values of the shape functions for two additional specimen sizes are calculated by using Eq. (14)

$$\Xi\left(\beta \,|\, W,\, \xi = -0.14\right) = 0.434 \cdot W^{0.14} \tag{19}$$

and the results are presented in Table 1. Note that $W = \{200, 1000\}$ [mm] values are the scaling-based predictions. The values of the Weibull moduli β, given in the third row of Table 1, are determined from Fig. 5d. In the light of $\Xi_{\min} = 0.73$ (Fig. 2), Eq. (19) implies the existence of $W_{\min} = 35$ mm, which represents the applicability threshold for the fracture toughness CDF (20) for the data set used in this numerical example. It is obvious from Eq. (14) that $W_{\min}$ is a threshold value characteristic of every experimental data set (since the parameters η_*, S_*, and ξ are data specific). In general, the condition $W > W_{\min}$ coincides with the characteristic sigmoid shape of the J_c CDF (by virtue of $\beta > \beta_\times = 1.35$ discussed with regards to Fig. 2).

Table 1.
Values of the shape function and the corresponding Weibull modulus for four different C(T) widths. The $W = \{200, 1000\}$ [mm] values are predictions based on the parameters determined by the scaling.

W [mm]	**50**	**100**	200	1000
Ξ [-]	0.77	0.845	0.93	1.17
β [-]	1.65	1.95	2.25	3.00

[4] Recall that the strength CDF of quasibrittle materials varies from Weibullian to Gaussian to as the structure size decreases [11].

[5] Due to the strong experimental data scatter, apparent in Fig. 5a, the values in this numerical example are limited to two significant digits with 0.5 rounding on the third.

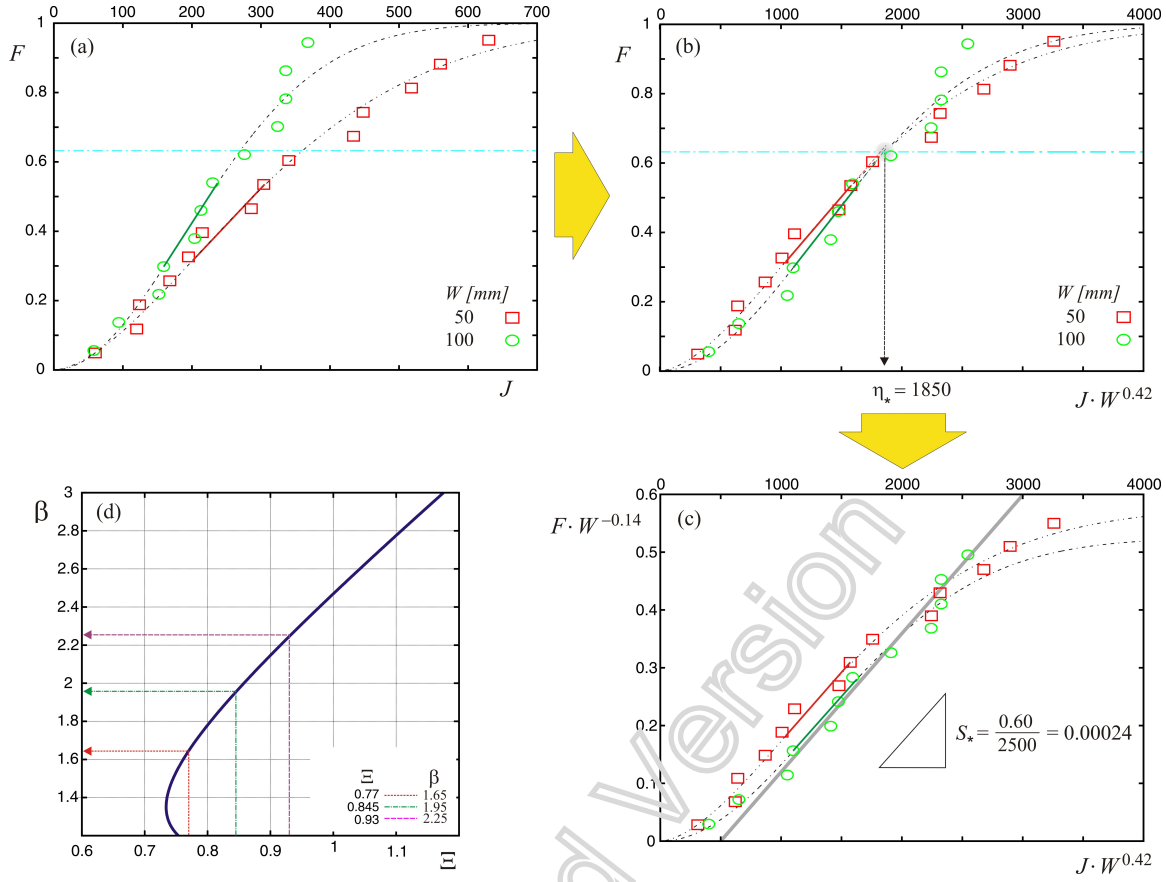

Fig. 5. The scaling procedure for the reactor steel 20MnMoNi55 at -60°C experimental data available from [13].

The Weibull CDF can now be written in the form

$$F(J \mid W) = 1 - \exp\left\{\left(\frac{J \cdot W^{0.42}}{1850}\right)^{\beta(W)}\right\}; \quad J \geq 0; W > W_{\min} = 35\,mm \tag{20}$$

where the size-dependent Weibull modulus $\beta(W)$ is defined in terms of Fig. 5d and Eq. (19). Note that, with the system-size increase Eq. (20) should be seen merely as a lower-bound approximation for C(T) tests on the reactor steel 20MnMoNi55 at temperature -60° C.

The results are illustrated in Fig. 6. With regards to Fig. 4 and the corresponding discussion, it could be argued that the blue dash-dot curve represents a satisfactory estimate of the J_c CDF for $W = 200$ mm while the purple dash-double dot curve represents a reasonable lower bound for $W = 1000$ mm.

4. Conclusions

A novel scaling algorithm is proposed to obtain an estimate of the J_c CDF for the reactor steel 20MnMoNi55 in the transition temperature region that takes into account the C(T) specimen linear dimension. The two-step scaling scheme is custom-developed and used on a very small experimental data set corresponding to the geometrically-similar C(T) specimen of only two effective widths $W = \{50, 100\}$ [mm] with {14, 12} data points per width, respectively. Such a small data set effectively limits the predictive capabilities of the analyst, especially when it comes to extrapolation of experimental results. The present scaling algorithm has been developed in an attempt to circumvent this difficulty in a systematic and transparent way. Due to the specific form of the two-parameter Weibull CDF, $F(J_c \mid \beta, \eta)$, this algorithm is applied according to a two-step scheme that defines the scaling parameters κ and ξ such that $\eta \cdot W^{\kappa} = const. = \eta_*$ and $S \cdot W^{\xi} = \text{const.} = S_*$.

The above-mentioned data set, involving only two specimen sizes, is used for nonlinear analysis. The findings demonstrate that:

- This novel scaling approach provides very good estimates in the intepolation range.
- The alghoritm ensures that a lower bound of the J_c CDF is obtained in the extrapolation range. The impact on applications is accentuated by the inherent reduction of reliability of the C(T) tests (in terms of the known sample-to-sample variability increase) for the miniscule and extremely large sample sizes.

- Depending on the limit value of the Weibull scale parameter for the unbounded system, η_∞ (driven by the system brittleness), this lower bound is a more or less conservative estimate of the J_c CDF for the most of the specimen-size range of the practical importance, which certainly exceeds the range of sizes that can be accurately tested.
- The obtained J_c CDF estimate comes with the applicability threshold in terms of the minimum specimen size ($W_{\min}$), which is a value specific of every experimental data set.

Certain aspects of the proposed scaling algorithm remain to be explored when more experimental data becomes available. A case in point is the optimization procedure for determination of the scaling parameters κ and ξ for data sets with more than two specimen widths. The application value of this novel approach—tailored for the experimental data sets of the statistical sizes that leave much to be desired—rests on the fact that it is not limited to any specific material or temperature range. In the present form it can be used whenever the Weibull distribution is applicable. The modification of the same analytical approach to other statistics remains a topic for a future research.

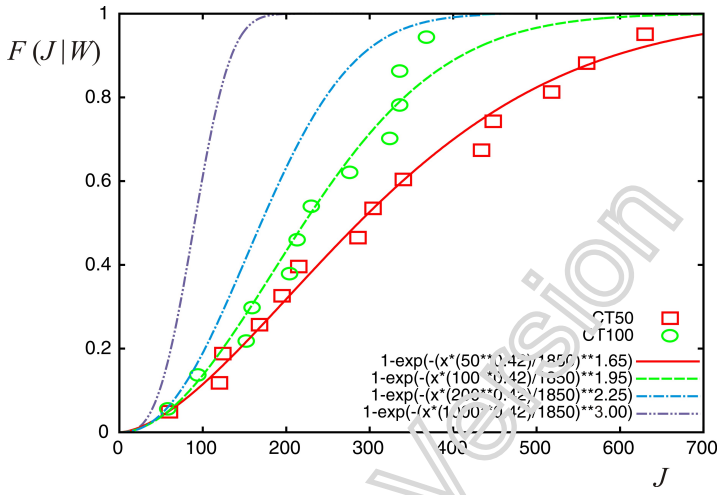

Fig. 6. Illustration of the results of the proposed scaling algorithm on the size effect on the J_c Weibull CDF for the reactor steel 20MnMoNi55, as given by Eq. (20) and shown in Table 1.

Declaration of Competing Interest

The authors declare that they have no known competing financial interests or personal relationships that could have appeared to influence the work reported in this paper.

Acknowledgment

This work was supported by the Ministry of Education, Science and Technological Development of the Republic of Serbia.

References

[1] Bažant, Z.P., Planas, J., *Fracture and Size Effect*, CRC Press, 1998.
[2] Bažant, Z.P., Chen, E.P., *Scaling of structural failure*, Applied Mechanics Reviews, 50: 593–627, 1997.
[3] Carpinteri, A., Chiaia, B., Ferro, G., *Multifractal scaling law for the nominal strength variations of concrete structures*. In: Size effect in concrete structures, Eds. Mihashi, M., Okamura, H., Bažant, Z., 1994.
[4] Duxbury, P.M., Beale, P.D., Leath, P.L., Size *effects of electrical breakdown in quenched random media*, Physical Review Letters, 57: 1052-1055, 1986.
[5] Herrmann, H.J., Hansen, A., Roux, S., *Fracture of disordered, elastic lattices in two dimensions*, Physical Review B, 39: 637-648, 1989.
[6] Jirasek, M., Bažant, Z.P., *Macroscopic fracture characteristics of random particle systems*, International Journal Fracture, 69: 201-228, 1995.
[7] Bolander, J.E., Hikosaka, H., He, W.-J., *Fracture in concrete specimens of different scale*, Engineering Computations, 15: 1094-1116, 1998.
[8] Mastilovic, S., *On strain-rate sensitivity and size effect of brittle solids: transition from cooperative phenomena to microcrack nucleation*. Continuum Mechanics and Thermodynamics 25: 489-501, 2013.
[9] Colpo A.B., Kosteski L.E., Iturrioz I., *The size effect in quasi-brittle materials: Experimental and numerical analysis*, International Journal of Damage Mechanics 26(3): 395–416, 2017.
[10] Kosteski, L.E., Iturrioz, I., Lacidogna, G., Carpinteri, A., *Size effect in heterogeneous materials analyzed through a lattice discrete element method approach*, Engineering Fracture Mechanics 232: 107041, 2020.
[11] Bažant, Z.P., Le, J-L., Bazant, M.Z., *Scaling of strength and lifetime probability distributions of quasibrittle structures based on atomistic fracture mechanics*, Proceedings of the National Academy of Sciences of the United States of America 106 (28): 11484-11489, 2009.
[12] Weibull, W., *A statistical theory of the strength of materials*, Journal of Applied Mechanics, 18: 293-297, 1951.
[13] Djordjevic, B., Sedmak, A., Petrovski, B., Dimic, A., *Probability distribution on cleavage fracture in function of Jc for reactor ferritic steel in transition temperature region*, Engineering Failure Analysis, 125: 105392, 2021.
[14] Ruggieri, C, Dodds Jr., R.H. *An engineering methodology for constraint corrections of elastic-plastic fracture toughness-Part I: A review on probabilistic models and exploration of plastic strain effects*. Engineering Fracture Mechanics 134:368-390, 2015.
[15] Shen, A., Li, P., Wang, K., Qian, G., Berto, F., *A simplified method for parameters calibration of the new local approach model for cleavage fracture in a ferritic steel*, Theoretical and Applied Fracture Mechanics 100: 426-433, 2019.
[16] Landes, J., McCabe, D., *Effect of Section Size on Transition Temperature Behavior of Structural Steels*, in Fracture Mechanics: Fifteenth Symposium, ed. R. Sanford (West Conshohocken, PA: ASTM International), 378-392, 1984.

[17] Landes, J., Zerbst, U., Heerens, J., Petrovski, B., Schwalbe, K., *Single-Specimen Test Analysis to Determine Lower-Bound Toughness in the Transition*, in Fracture Mechanics: Twenty-Fourth Volume, ed. J. Landes, D. McCabe, and J. Boulet (West Conshohocken, PA: ASTM International), 171-185, 1994.
[18] Beremin, F.M., Pineau, A., Mudry, F., Devaux, J-C., D'Escatha, Y., Ledermann, P., *A local criterion for cleavage fracture of a nuclear pressure vessel steel,* Metallurgical Transactions A 14: 2277–2287, 1983.
[19] Pineau, A., *Development of the local approach to fracture over the past 25 years: Theory and applications*. International Journal of Fracture 138: 139–166, 2006.
[20] Qian, G., Lei, W-S., Tong, Z., Yu, Z., *A Statistical Model of Cleavage Fracture Toughness of Ferritic Steel DIN 22NiMoCr37 at Different Temperatures*, Materials 12: 982, 2019, doi:10.3390/ma12060982
[21] Wallin, K., *The Master Curve Method: A New Concept for Brittle Fracture*, International Journal of Materials and Product Technology 14: 342–354, 1999.
[22] Wallin, K., *Master curve analysis of the "Euro" fracture toughness dataset.* Engineering Fracture Mechanics 69: 451–481, 2002.
[23] ASTM E1921 – 10, *Standard Test Method for Determination of Reference Temperature, T_0, for Ferritic Steels in the Transition Range*. Annual Book of ASTM standards, ASTM International, Philadelphia, USA, 2010.
[24] ASME Code Case N-830, *Direct Use of Master Fracture Toughness Curve for Pressure-Retaining Materials of Class 1 Vessels Section XI,* ASME Boiler & Pressure Vessel Code, Code Cases: Nuclear Components, American Society of Mechanical Engineers, New York, USA, 2014.
[25] International Atomic Energy Agency (IAEA). *Guidelines for Applications of the Master Curve Approach to Reactor Pressure Vessel Integrity in Nuclear Power Plants;* Technical Reports Series No.429; International Atomic Energy Agency: Vienna, Austria, 91–95, 2005.
[26] Margolin, B., Shvetsova, V., Kostylev, V., *Radiation embrittlement modelling in multi-scale approach to brittle fracture of RPV steels*. International Journal of Fracture 179: 87–103, 2013.
[27] Lei,W-S., *A cumulative failure probability model for cleavage fracture in ferritic steels*, Mechanics of Materials 93: 184–198, 2016a.
[28] Lei,W-S., *On the statistical modeling of cleavage fracture toughness of structural steels*, Mechanics of Materials 101: 81–92, 2016b.
[29] Meshii, T., *Failure of the ASTM E 1921 master curve to characterize the fracture toughness temperature dependence of ferritic steel and successful application of the stress distribution T-scaling method*, Theoretical and Applied Fracture Mechanics 100: 354-361, 2019.
[30] Paul, S., Dey, P., Bhattacharjee, S., Acharya, S.K., Sahoo, P.,Chattopadhyay, J., *Phenomenological modelling of flow behaviour of 20MnMoNi55 reactor pressure vessel steel at cryogenic temperature with different strain rates*, Defence Technology 15: 336-337, 2019.
[31] Yoshimura, S., Kaito, Y. *Probabilistic Fracture Mechanics for Risk-Informed Activities – Fundamentals and Application*, Atomic Energy Research Committee, The Japan Welding Engineering Society, Tokyo, Japan, 2020. ISBN 978-4-907200-07-7.
[32] Stauffer, D., Aharony, A., *Introduction to Percolation Theory*, Taylor & Francis, 1992.
[33] Djordjevic, B., Sedmak, A., Petrovski, B., Dimic, A., *Weibull probability distribution for reactor steel 20MnMoNi55 cleavage fracture in transition temperature*, Procedia Structural Integrity 28: 295-300, 2020.
[34] Krajcinovic, D., Rinaldi, A., *Statistical Damage Mechanics – 1. Theory,* Journal of Applied Mechanics - Transactions of the ASME, 72: 76–85, 2005.
[35] Rinaldi A., Mastilovic S., *The Krajcinovic Approach to Model Size Dependent Fracture in Quasi-Brittle Solids*, Mechanics of Materials, 71: 21-33, 2014.
[36] Mastilovic, S., *Some Sigmoid and Reverse-Sigmoid Response Patterns Emerging From High-Power Loading of Solids*, Theoretical and Applied Mechanics 45(1): 95-119, 2018.
[37] Herrmann, H.J., *Introduction to basic notions and facts*. In: Statistical Models for the Fracture of Disordered Media (Eds. Herrmann H.J. and Roux, S.). North Holland, 1990.
[38] Nishimori, H., Ortiz, G., *Elements of Phase Transitions and Critical Phenomena*, Oxford University Press, 2011.
[39] Mastilovic, S., *Damage-fragmentation transition: Size effect and scaling behavior for impact fragmentation of slender projectiles*, International Journal of Damage Mechanics 27 (2): 201-217, 2018.
[40] Jose, N.M., Chattopadhyay, J., Durgaprasad, P.V., Naveen Kumar, V., *Master Curve of 20MnMoNi55Steel from Miniature CT Specimens*, Procedia Structural Integrity 14: 403-409, 2019.